the solution composition; we obtained $T_{2e} \simeq 2 \times 10^{-9}$ s at room temperature, which agreed with the reported value for manganese(II) in dilute aqueous solution.[29,30] In our case, $\omega_s$ is $2.48 \times 10^{11}$ rad $s^{-1}$, and $\tau_M$ is about $10^{-8}$ s at room temperature. Generally, $\tau_r$ is nearly equal to $10^{-11}$ s.[31,32] Therefore, suppose that $T_{1e}^{-1} = T_{2e}^{-1}$; then $(1/T_2)_{HF} = C_{HF}T_{2e}$. With our experimental value of $C_\omega = 2.4 \times 10^6$ K rad $s^{-1}$ for the methyl protons, we obtain $A = 4.6 \times 10^{-22}$ erg and $C_{HF} = 5.5 \times 10^{11}$ $s^{-2}$. Since the estimated value of $(1/T_2)_{HF}$ is much smaller than the observed value of $1/T_{2M}$, we conclude that $T_{2M}^{-1} = (1/T_2)_{DD}$, i.e. the mechanism of $T_{2M}$ is the dipole-dipole interaction, and also that is the case for the hydroxyl proton. Since there is a linear relationship between log $T_{2M}^{-1}$ and $1/T$ in the higher temperature region as apparent from Figure 1, we can represent $T_{2M}^{-1}$ as an exponential function (vide supra). The electron-proton distance $r$ estimated by using eq 4 is ca. 3.8 Å, which seems to be a reasonable distance. This value is similar to that for the hydroxyl proton since the values of $T_{2M}^{-1}$ for both protons are alike.

**Acknowledgment.** The authors are indebted to Mr. T. Seto, Nagoya University, for performing the ESR measurements. This work was partially supported by Grant-in-Aid for Developmental Scientific Research (No. 00584023) from the Japanese Ministry of Education, Science, and Culture.

**Registry No.** HOAc, 64-19-7; Mn, 7439-96-5; $[Mn(HOAc)_6](ClO_4)_2$, 20298-15-1.

**Supplementary Material Available:** Experimental proton line broadening and proton chemical shift data for $Mn(ClO_4)_2$ in acetic acid and in mixtures with inert solvents (Table sI) and values of $C_M$, $E_M$, $C_O$, and $E_O$ (Table sII) (4 pages). Ordering information is given on any current masthead page.

(29) Tinkham, M.; Weinstein, R.; Kip, A. F. *Phys. Rev.* **1951**, *84*, 848.
(30) Schneider, E. E.; England, T. S. *Physica (Amsterdam)* **1951**, *17*, 221.
(31) Broersma, S. *J. Chem. Phys.* **1956**, *24*, 659.
(32) Johnson, K. J.; Hunt, J. P.; Dodgen, H. W. *J. Chem. Phys.* **1969**, *51*, 4493.

Contribution from the Department of Chemistry, University of California, Riverside, California 92521, and the Division of Chemistry and Chemical Engineering, California Institute of Technology, Pasadena, California 91125

# Structural Characterization of Tris(3,5-di-*tert*-butylcatecholato)manganate(IV) and Its Redox Reactions with Superoxide Ion

DER-HANG CHIN,[1a] DONALD T. SAWYER,*[1a] WILLIAM P. SCHAEFER,*[1b] and CHARLES J. SIMMONS[1b,c]

*Received February 10, 1982*

The disodium salt of the tris(catecholato) complex of manganese(IV), $[Na_2Mn^{IV}(DTBC)_3 \cdot 6MeCN]$, has been synthesized and isolated as dark blue irregular crystals. The structure of the complex, as determined by single-crystal X-ray diffraction methods (hexagonal, $R\bar{3}$; $a = 14.548$ (6) Å, $c = 49.731$ (9) Å; $Z = 6$), is a nearly symmetric octahedral array of oxygen donor atoms (from the three catechol ligands) about the manganese(IV) ion. The proton and $^{13}C$ NMR spectra for the complex in $Me_2SO$-$d_6$ and pyridine-$d_5$ indicate that it maintains its main structural features in solution. The reactions of the blue $Mn^{IV}(DTBC)_3^{2-}$ complex and its green reduction product, $Mn^{III}(DTBC)_2(H_2O)_2^-$, with superoxide ion in aprotic media have been characterized by spectroscopic, magnetic, and electrochemical studies.

Manganese is an essential cofactor of green-plant photosynthesis in photosystem II for the oxidation of water to dioxygen.[2-4] Another important biological role is as the active catalytic center in mitochondrial and several bacterial superoxide dismutases.[5-7] Apoenzyme that is reconstituted with Fe(II), Co(II), Ni(II), and Cu(II) does not exhibit catalytic activity,[8,9] but reconstitution with $MnCl_2$ restores full catalytic activity.[9] In reactions with photosystem II, manganese appears to serve as an electron-transfer agent in the charge accumulation center of the water oxidizing system. Its other probable role is as a template to bring the oxygen atoms of two water molecules into close proximity to form an O–O bond.[4] Although quinones are present in significant quantities in chloroplasts,[10] they are not effective ligands for transition-metal ions. A model for the manganese cofactor of photosystem II has been proposed that makes use of manganese–catechol complexes as templates for the formation of O–O bonds.[4] This has prompted preparation of stable manganese–catechol complexes to act as effective models for the manganese cofactor of photosystem II and for manganese superoxide dismutases.

In a previous study we observed that molecular oxygen is reversibly bound by the tris(3,5-di-*tert*-butylcatecholato)manganate(IV) complex in aprotic media.[11,12] Because this process is equivalent to the terminal step of the photosystem II oxygen evolution reaction, the structural characterization of the complex and its dioxygen adduct is desirable. The present report summarizes the results of a single-crystal X-ray diffraction study of the tris(3,5-di-*tert*-butylcatecholato)manganate(IV) complex. Its reactions with dioxygen and superoxide ion as well as those for the bis(3,5-di-*tert*-butylcatecholato)manganate(III) complex have been characterized and provide reasonable insight into the mechanism for the

(1) (a) University of California. (b) California Institute of Technology. (c) Present address: Department of Chemistry, Texas A&M University, College Station, TX 77843.
(2) (a) Heath, R. L. *Int. Rev. Cytol.* **1973**, *34*, 49. (b) Bearden, A. J.; Malkin, R. *Q. Rev. Biophys.* **1975**, *7*, 131.
(3) Radmer, R.; Cheniae, G. M. "Primary Processes"; Elsevier-North Holland: New York, 1977; Vol. 2.
(4) Lawrence, G. L.; Sawyer, D. T. *Coord. Chem. Rev.* **1978**, *27*, 173.
(5) Michelson, A. M., McCord, J. M., Fridovich, I., Eds. "Superoxide and Superoxide Dismutase"; Academic Press: New York, 1977.
(6) Weisiger, R. A.; Fridovich, I. *J. Biol. Chem.* **1973**, *248*, 3582.
(7) Ravindrath, S. D.; Fridovich, I. *J. Biol. Chem.* **1975**, *250*, 6107.
(8) Ose, D. E.; Fridovich, I. *J. Biol. Chem.* **1976**, *251*, 1217.
(9) Brock, C. J.; Harris, J. I. *Biochem. Soc. Trans.* **1977**, *5*, 1537.
(10) Lichtenthler, H. K. *Prog. Photosynth. Res., Proc. Int. Congr. [1st]* **1969**, 304.
(11) Magers, K. D.; Smith, C. G.; Sawyer, D. T. *Inorg. Chem.* **1980**, *19*, 492.
(12) Magers, K. D.; Smith, C. G.; Sawyer, D. T. *J. Am. Chem. Soc.* **1978**, *100*, 989.

0020-1669/83/1322-0752$01.50/0 

reversible dioxygen binding process.

## Experimental Section

**Chemicals and Reagents.** The reagents for the studies included $Mn^{II}(ClO_4)_2 \cdot 6H_2O$ (G. Frederick Smith), 3,5-di-*tert*-butylcatechol ($DTBCH_2$) (Aldrich), 3,5-di-*tert*-butyl-*o*-benzoquinone (DTBQ) (Aldrich), tetraethylammonium perchlorate (TEAP) (G. Frederick Smith), sodium sulfate anhydrous (Mallinckrodt), sodium hydroxide (Mallinckrodt), methanol (spectrophotometric grade; Mallinckrodt), tetramethylammonium hydroxide pentahydrate (Southwestern Analytical Chemicals), potassium superoxide (Alfa Products), and ammonia (Matheson). The aprotic solvents included acetonitrile, dimethylformamide, and dimethyl sulfoxide ($Me_2SO$); these were obtained from Burdick and Jackson ("distilled in glass") in quart bottles to minimize contamination by water. Voltammetric scans confirmed that the solvents were free of electroactive impurities. Pyridine-$d_5$ and dimethyl-$d_6$ sulfoxide were supplied by Aldrich and were dried with activated Type 4-A molecular sieves (Matheson Coleman and Bell). Acetonitrile-$d_3$ (Aldrich) was dried with sodium sulfate (anhydrous) in the glovebox. Superoxide ion was introduced into solutions as the tetramethylammonium salt ($(TMA)O_2$), which was synthesized from the combination of $KO_2$ and $(TMA)OH \cdot 5H_2O$ followed by extraction into liquid ammonia. Superoxide ion also was generated by the electrochemical reduction of a solution through which oxygen (at 1 atm) was continuously bubbled. All electrochemical solutions contained 0.1 M tetraethylammonium perchlorate (TEAP) as the supporting electrolyte. Upon completion of the electrolysis, the superoxide solution was degassed with argon to remove any residual oxygen. The concentration of superoxide ion was monitored by the voltammetric anodic peak current at −0.7 V vs. SCE. Standardization of the current relative to the concentration of superoxide ion was accomplished by controlled-potential coulometric analysis.

**Synthesis of $Na_2Mn^{IV}(DTBC)_3 \cdot 6MeCN$ and $NaMn^{III}(DTBC)_2 \cdot 4MeCN$.** The crystals of the disodium salt of tris(3,5-di-*tert*-butylcatecholato)manganate(IV) were prepared from the stoichiometric combination of NaOH, $DTBCH_2$, DTBQ, and $Mn^{II}(ClO_4)_2 \cdot 6H_2O$ in MeCN by a previously described synthetic procedure.[13] The same reagents were used to prepare the needlelike crystals of the sodium salt of bis(3,5-di-*tert*-butylcatecholato)manganate(III) complex. For the latter synthesis 1.8 g of $Mn^{II}(ClO_4)_2 \cdot 6H_2O$ was mixed with 2.2 g of $DTBCH_2$ in 50 mL of MeCN in an inert-atmosphere box. To this mixture was added dropwise 5 mL of 2 M NaOH (in MeOH) while the solution was stirred vigorously. This produced a pink precipitate of $Mn^{II}(DTBC)$, which was separated by filtration and washed with 5–10 mL of MeCN. To this precipitate in 50 mL of MeCN was added 0.55 g of $DTBCH_2$, followed by the dropwise addition of 2.5 mL of 2 M NaOH (in MeOH). Upon the addition of 0.55 g of DTBQ, the solution became dark green due to the formation of the bis(3,5-di-*tert*-butylcatecholato)manganate(III) complex. Anhydrous $Na_2SO_4$ was added as a drying agent, and the solution was stirred and warmed for 30 min prior to filtration. After 12 h dark brown crystals formed in the filtrate. These were separated by filtration and recrystallized from MeCN and anhydrous $Na_2SO_4$. Because these crystals were prone to lose solvent molecules and decompose to a green powder, care had to be taken during the filtration process. The elemental microanalysis for the isolated material indicated that the complex has the formula $NaMn^{III}(DTBC)_2 \cdot 4MeCN$. Anal. Calcd for $NaMnC_{36}H_{52}O_4N_4$: C, 63.34; H, 7.62; O, 9.38; Mn, 8.06; Na, 3.37; N, 8.21. Found: C, 62.32; H, 7.44; O, 10.13; Mn, 7.88; Na, 3.76; N, 8.59 (Galbraith Laboratories, Inc.).

**Single-Crystal X-ray Diffraction Measurements of $Na_2Mn^{IV}(DTBC)_3 \cdot 6MeCN$.** Because crystals of $Na_2Mn^{IV}(DTBC)_3 \cdot 6MeCN$ are unstable in the presence of air and moisture and are prone to lose their solvent molecules, they were mounted in capillaries in a dry nitrogen atmosphere that was saturated with MeCN.

Preliminary photographs and diffractometer data (graphite-monochromated Mo K$\alpha$ radiation) indicated a hexagonal cell. The only condition for systematic absences, $-h + k + l \neq 3n$, and the Laue symmetry, $\bar{3}$, are consistent only with space groups $R3$ and $R\bar{3}$. A complete data set was collected, and the manganese atoms were positioned. The structure could not be solved in $R3$, but a disordered structure in $R\bar{3}$ was refined to an $R$ index of 0.072. However, there were two impossibly short carbon–carbon contacts in this model that could only be eliminated by assuming the disorder was highly systematic—sufficiently so as to cause the $c$ axis to be doubled. More photographs confirmed this; there were weaker lines corresponding to the larger cell clearly visible. A new crystal was mounted, and a new data set was collected on a Syntex $P2_1$ diffractometer. The irregular crystal measured 0.31 × 0.23 × 0.15 mm. The cell dimensions given in Table I were determined by least squares from the angular coordinates of 15 reflections, representing various forms of three independent reflections with $20° \leq 2\theta \leq 22°$.

**Table I.** Crystal Data

| | |
|---|---|
| formula: $Na_2Mn(C_{14}H_2O_2)_3 \cdot 6CH_3C{\equiv}N$ | fw 1008.18 |
| space group: $R\bar{3}$ (No. 148) | $V = 9116$ (5) Å$^3$ |
| $a = 14.548$ (6) Å | $Z = 6$ |
| $c = 49.731$ (9) Å ($T = 21$ °C) | $\rho$(calcd) = 1.102 g cm$^{-3}$ |
| $\lambda$(Mo K$\bar{\alpha}$) = 0.710 69 Å | $\mu$(Mo K$\bar{\alpha}$) = 2.91 cm$^{-1}$ |
| $F(000) = 3234$ e | $\mu r_{max} = 0.12$ |

A total of 7854 reflections with $2\theta < 40°$ was measured by $\theta$–$2\theta$ scan technique at a scan speed of 1°/min in $2\theta$, with a background time:scan time ratio of 1.0. Four check reflections were measured every 100 reflections. These showed decays of 1%–3% in $F$ over the 278 h that was needed to collect the data. The data were corrected for this decay and for Lorentz and polarization factors. No absorption correction was applied. Careful examination of the scans indicated that many of those which were collected later were highly asymmetric, presumably because the crystal had moved slightly. The problems were confined to certain volumes of reciprocal space, but because the boundaries could not be defined precisely, we eliminated the last 2654 reflections from the data set. The remainder were combined to give 1871 independent reflections, most of which had been measured in three forms; 1896 reflections were possible below a $2\theta$ of 40°. Of the 1871 reflections, 1616 were greater than zero, but only 889 had $F_o^2 > 3\sigma(F_o^2)$, reflecting the fact that about half the data have $l$ odd and are systematically weak. Variances, $\sigma^2(I)$, were assigned the intensities on the basis of counting statistics with an additional term, $(0.02I)^2$, to account for additional errors proportional to the intensity. All 1871 reflections were used in the refinement of the structure. Atomic scattering factors for $Mn^{2+}$, Na, N, O, C, and H (bonded) were used;[14] those for $Mn^{2+}$ and Na were modified to include both the real and imaginary parts of the anomalous dispersion correction.[15]

The heavy-atom parameters from the first refinement were transformed to correspond to the new cell. Refinement by least squares converged with the $R$ index = 0.132 and the goodness of fit = 2.48 ($R = \sum||F_o| - |F_c||/\sum F_o$; GOF = $[\sum w(F_o^2 - F_c^2)^2/(n-p)]^{1/2}$). Hydrogen atoms were added at calculated positions or (for the methyl hydrogens) at optimized positions determined from difference maps calculated in the planes where they were expected. The C–H distance used was 0.9 Å. The hydrogen atoms were repositioned three times after further refinement of the heavy-atom parameters. The final cycles of least squares had the heavy-atom coordinates in one matrix and the temperature factors (isotropic for the six carbon atoms of the catechol ring, anisotropic for the remaining atoms) and the scale factor in another matrix. The hydrogen atoms were included as fixed contributions. In the final cycle, no parameter shifted by more than 25% of its standard deviation. The final $R$ index for all reflections with $F_o^2 > 0$ is 0.120; for $F_o^2 > 3\sigma(F_o^2)$, it is 0.066. the final difference map showed maximum excursions of ±0.7 e Å$^{-3}$. Final parameters are given in Table II.

Calculations were done by using the programs of the CRYM crystallographic computing system[16] on an IBM 370/3032 and a VAX11/780 computer. The drawings were done by using ORTEP.[17]

**Instrumentation.** A Princeton Applied Research Model 173/175/179 potentiostat–galvanostat was used for the cyclic voltammetric experiments. The voltammograms were recorded with a Houston

(13) Jones, S. E.; Chin, D.-H.; Sawyer, D. T. *Inorg. Chem.* **1981**, *20*, 4257.

(14) (a) "International Tables for X-Ray Crystallography"; Kynoch Press: Birmingham, England, 1962; Vol. III, p 202. (b) For hydrogen: Stewart, R. F.; Davidson, E. R.; Simpson, W. T. *J. Chem. Phys.* **1965**, *42*, 3175.

(15) Cromer, D. T. *Acta Crystallogr.* **1965**, *18*, 17.

(16) Duchamp, D. J. paper presented at the Regional Meeting of the American Crystallographic Association, Bozeman, MT, 1964; No. B19, p 29.

(17) Johnson, C. D. "ORTEP, a Fortran Thermal Ellipsoid Plot Program" Report ORNL-3794; Oak Ridge National Laboratory: Oak Ridge, TN, **1965**.

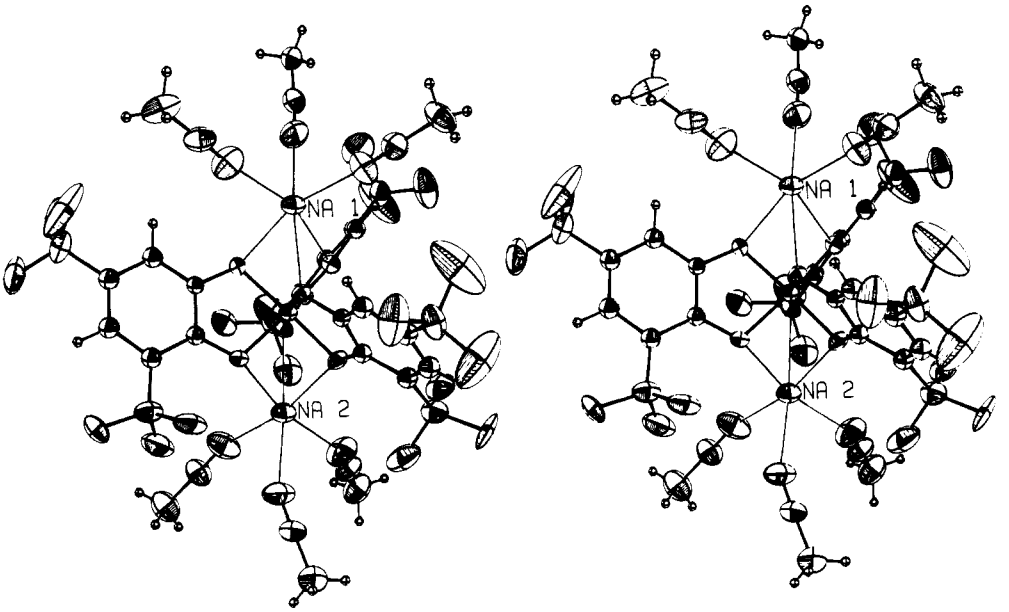


**Figure 1.** ORTEP drawing, roughly perpendicular to the threefold axis, showing the atoms in the asymmetric unit. Thermal ellipsoids are set at the 25% probability level; hydrogen atoms are given arbitrary $B$ values of 1.0 Å$^2$. Hydrogen atoms on the *tert*-butyl groups were left out for clarity.

**Table II.** Final Positional and Thermal Parameters[a]

| atom | $x$ | $y$ | $z$ | $U_{eq}$[b] or $B$, Å$^2$ | pop.[c] |
|---|---|---|---|---|---|
| Mn | 0 | 0 | 2502 (1) | 0.0380 (2) | 6 |
| Na1 | 0 | 0 | 1881 (1) | 0.0572 (9) | 6 |
| Na2 | 0 | 0 | 3104 (1) | 0.0630 (9) | 6 |
| O1 | 621 (4) | 1207 (4) | 2282 (1) | 0.0373 (12) | 18 |
| O2 | −447 (4) | 774 (4) | 2717 (1) | 0.0408 (11) | 18 |
| C1 | 361 (5) | 1922 (6) | 2358 (1) | 3.5 (2) | 18 |
| C2 | −252 (6) | 1678 (6) | 2591 (2) | 4.0 (2) | 18 |
| C3 | −630 (6) | 2365 (6) | 2671 (2) | 4.7 (2) | 18 |
| C4 | −310 (6) | 3281 (6) | 2519 (2) | 5.0 (2) | 18 |
| C5 | 350 (6) | 3546 (7) | 2302 (2) | 5.0 (2) | 18 |
| C6 | 668 (6) | 2853 (7) | 2215 (2) | 4.8 (2) | 18 |
| C7 | −1381 (8) | 2126 (9) | 2902 (2) | 0.077 (3) | 18 |
| C8 | −2323 (9) | 1030 (10) | 2879 (2) | 0.092 (3) | 18 |
| C9 | −1780 (9) | 2924 (9) | 2942 (2) | 0.077 (2) | 18 |
| C10 | −823 (9) | 2153 (10) | 3165 (2) | 0.113 (4) | 18 |
| C11 | 683 (9) | 4576 (8) | 2140 (3) | 0.084 (3) | 18 |
| C12 | 1797 (11) | 5101 (9) | 2067 (3) | 0.151 (4) | 18 |
| C13 | 437 (15) | 5319 (11) | 2273 (4) | 0.181 (5) | 18 |
| C14 | 90 (14) | 4277 (11) | 1884 (4) | 0.281 (9) | 18 |
| N1 | 1095 (10) | 1514 (10) | 3416 (2) | 0.115 (4) | 18 |
| CN11 | 1140 (10) | 2017 (11) | 3584 (3) | 0.082 (4) | 18 |
| CN12 | 1185 (9) | 2685 (10) | 3796 (2) | 0.106 (4) | 18 |
| N2 | −509 (9) | 1090 (9) | 1602 (3) | 0.103 (4) | 18 |
| CN21 | −739 (9) | 1531 (11) | 1455 (3) | 0.084 (4) | 18 |
| CN22 | −1104 (8) | 2100 (9) | 1266 (2) | 0.109 (4) | 18 |

[a] Positional parameters have been multiplied by $10^4$. [b] $U_{eq} = {}^1/_3U_{33} + {}^4/_9(U_{11} + U_{22} - 2U_{12})$; $\sigma(U_{eq}) = (1/6^{1/2})\langle\sigma(U_{ii})/U_{ii}\rangle U_{eq}$. [c] The number of atoms in the unit cell.

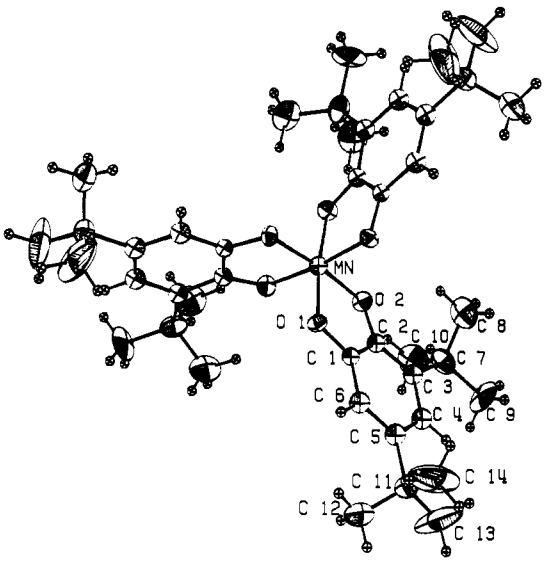


**Figure 2.** ORTEP view down the threefold axis, showing the anion and the atom-numbering system. Thermal ellipsoids are set at the 25% probability level; hydrogen atoms are given arbitrary $B$ values of 1.0 Å$^2$.

Instruments Omnigraph X-Y recorder. The working electrode was a Beckman platinum-inlay electrode (No. 39273), which had a surface area of 0.23 cm$^2$. The auxiliary electrode was a platinum-flag electrode, which was isolated from the bulk solution by a fine- or a medium-pososity glass frit. The reference electrode was located inside a Luggin capillary (filled with solvent solution) in the cell assembly.[18]

NMR spectra were obtained at 95.5 MHz on a modified multinuclear Bruker WH90-18 (18-in., 2.11-T magnet) NMR spectrometer. The magnetic susceptibility measurements were made with a Varian EM-390 NMR spectrometer by the Evans method[19-21] as modified by Rettig.[22] ESR data were obtained with a Varian Model V-4500 spectrophotometer. Cary Model 17D and Model 219 spectrophotometers were used for the UV–visible spectrophotometric measurements.

## Results

**Crystal Structure of $Na_2Mn^{IV}(DTBC)_3\cdot 6MeCN$.** The structure consists of dinegative Mn(IV) complex anions located on threefold axes with sodium cations above and below the manganese atom, 3.085 (6) and 2.996 (6) Å away. The solvent molecules, six per anion, are above and below the sodium atoms, with the nitrogen atoms directed toward the sodium atom at an average Na–N distance of 2.49 (1) Å. There are no distances between anions or solvent molecules shorter than van der Waals contacts. Figure 1 is a stereoview of the molecule.

(18) Goolsby, A. D.; Sawyer, D. T. *Anal. Chem.* **1967**, *39*, 411.
(19) Evans, D. F. *J. Chem. Soc.* **1959**, *2003*.
(20) Crawford, T. H.; Swanson, J. *J. Chem. Educ.* **1971**, *43*, 382.
(21) Ostfeld, D.; Cohen, I. A. *J. Chem. Educ.* **1972**, *49*, 829.
(22) Rettig, M. F., University of California, Riverside, CA, private communication.

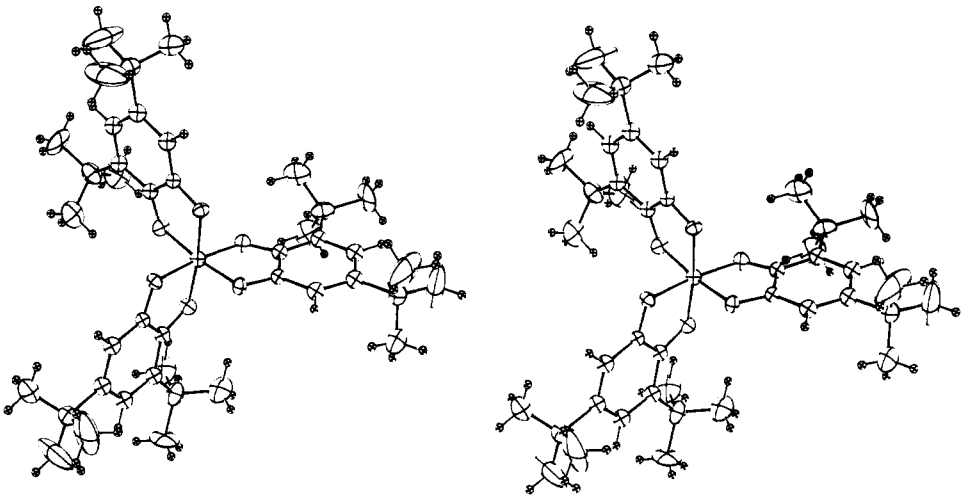

**Figure 3.** ORTEP view down the threefold axis, showing the manganese anion. Thermal ellipsoids are set at the 25% probability level; hydrogen atoms are given arbitrary $B$ values of 1.0 Å$^2$.

**Table III.** Distances (Å) and Angles (deg)

| | | | |
|---|---|---|---|
| | | Distances | |
| Mn-O1 | 1.874 (6) | C7-C9 | 1.548 (16) |
| Mn-O2 | 1.891 (6) | C7-C10 | 1.528 (17) |
| O1-C1 | 1.327 (10) | C5-C11 | 1.548 (15) |
| O2-C2 | 1.353 (10) | C11-C12 | 1.450 (19) |
| C1-C2 | 1.399 (12) | C11-C13 | 1.458 (22) |
| C2-C3 | 1.417 (12) | C11-C14 | 1.479 (22) |
| C3-C4 | 1.393 (12) | N1-CN11 | 1.094 (20) |
| C4-C5 | 1.369 (12) | CN11-CN12 | 1.412 (19) |
| C5-C6 | 1.372 (12) | N2-CN21 | 1.130 (19) |
| C6-C1 | 1.390 (12) | CN21-CN22 | 1.513 (18) |
| C3-C7 | 1.502 (14) | | |
| C7-C8 | 1.499 (17) | | |
| | | Angles | |
| O1-Mn-O2 | 85.5 (3) | C3-C7-C9 | 115.3 (9) |
| Mn-O1-C1 | 112.0 (5) | C3-C7-C10 | 109.4 (9) |
| Mn-O2-C2 | 110.4 (5) | C8-C7-C9 | 108.8 (9) |
| O1-C1-C2 | 115.7 (7) | C8-C7-C10 | 106.5 (10) |
| O2-C2-C1 | 115.4 (7) | C9-C7-C10 | 105.3 (9) |
| O1-C1-C6 | 122.7 (7) | C4-C5-C11 | 121.2 (8) |
| O2-C2-C3 | 126.1 (8) | C6-C5-C11 | 119.4 (8) |
| C1-C2-C3 | 118.5 (8) | C5-C11-C12 | 111.5 (10) |
| C2-C3-C4 | 117.4 (8) | C5-C11-C13 | 114.3 (11) |
| C3-C4-C5 | 123.4 (8) | C5-C11-C14 | 108.0 (11) |
| C4-C5-C6 | 119.2 (8) | C12-C11-C13 | 110.4 (12) |
| C5-C6-C1 | 119.6 (8) | C12-C11-C14 | 105.8 (12) |
| C6-C1-C2 | 121.7 (8) | C13-C11-C14 | 106.4 (13) |
| C2-C3-C7 | 123.0 (8) | N1-CN11-CN12 | 178.0 (16) |
| C4-C3-C7 | 119.5 (8) | N2-CN21-CN22 | 176.9 (15) |
| C3-C7-C8 | 111.1 (9) | | |

An isolated anion is shown in Figure 2. The complex has a nearly perfect octahedral geometry with Mn–O distances of 1.874 (6) and 1.891 (6) Å and O–O distances of 2.556 (8), 2.635 (8), 2.697 (8), and 2.765 (8) Å. The O–Mn–O angles range from 85.5 ( 3) to 94.5 (3)°; the trans angle is 173.5 (3)°. The one independent 3,5-di-*tert*-butylcatecholato ligand has normal distances and angles (Table III). The carbon atoms of the benzene ring have small thermal parameters, while the carbon atoms of the *tert*-butyl groups have much larger anisotropic motions (Table II). In general, their principal axes are aligned perpendicular to the C–C bonds. These large thermal motions are mirrored in the short C–C distances observed for the *tert*-butyl groups, especially the C11–C12, –C13, and –C14 distances. The angles of the *tert*-butyl groups show an average deviation of 1.2 (22)° from 109.5°. Figure 3 is a stereoview of the anion.

**Proton NMR Spectra of $Na_2Mn^{IV}(DTBC)_3$.** The Mn(IV) complex exhibits similar NMR spectra in deuterated $Me_2SO$, pyridine, and acetonitrile. For proton NMR there is a single large sharp *tert*-butyl proton peak at approximately 2 ppm (downfield relative to $Me_4Si$) plus a broad, weak phenyl proton resonance upfield at approximately −35 ppm vs. $Me_4Si$. The effect of temperature on these proton resonances is illustrated by Figure 4. Broad-band decoupled $^{13}C$ NMR spectra of $Na_2Mn^{IV}(DTBC)_3$ in pyridine and $Me_2SO$ exhibit a *tert*-butyl resonance at 0.7 ppm (downfield relative to $Me_4Si$). Unlike the $^{13}C$ spectral resonances for free $DTBCH_2$ or DTBQ, this is a single peak (the same is true for the $^1H$ NMR spectra).

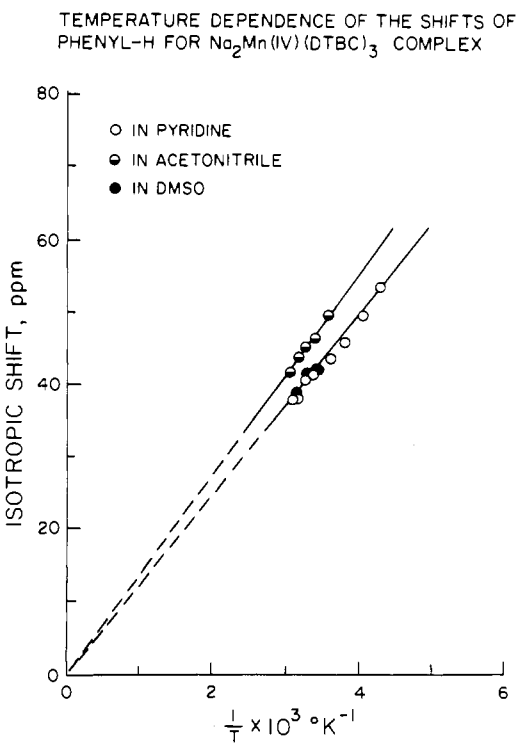


**Figure 4.** Curie plot for the proton NMR chemical shifts of $Mn^{IV}(DTBC)_3^{2-}$ as a function of temperature.

**Reactions of $Mn^{III}(DTBC)_2^-$ with Superoxide Ion.** The electronic spectrum of $Mn^{III}(DTBC)_2^-$ in MeCN exhibits two shoulders at 375 and 335 nm plus peaks at 285, 240, and 210 nm (see Figure 5). When 1 equiv of superoxide ion is added to the green solution, it immediately changes to a blue color (absorption peak at 590 nm). When excess superoxide is added, the solution becomes red-brown with an absorption peak at 450 nm. When oxygen is introduced, the red-brown species is converted to a blue species (absorption at 590 nm). Under

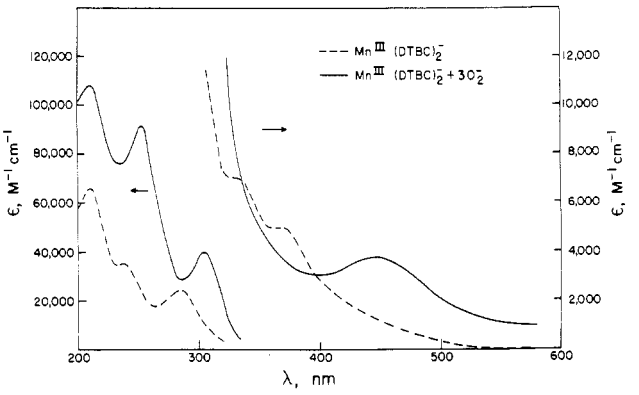


**Figure 5.** Electronic spectra in MeCN for the green $Mn^{III}(DTBC)_2(H_2O)_2^-$ complex and for the product solution that results from its combination with $O_2^-$. Molar absorptivities are relative to total manganese concentration.

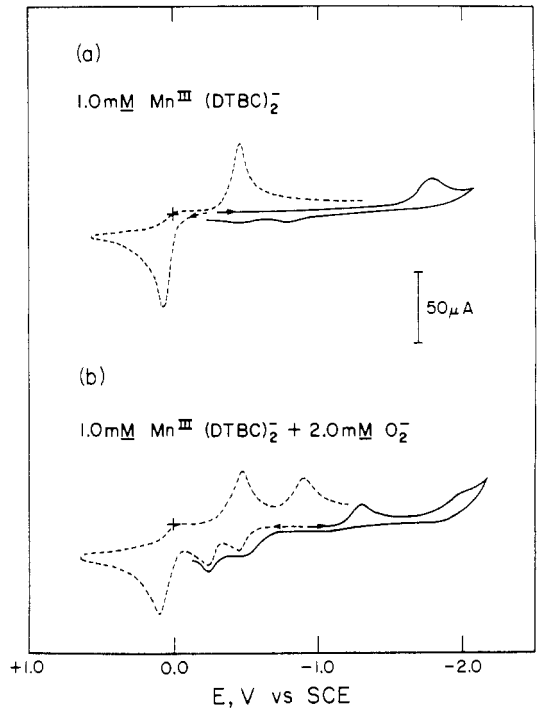


**Figure 6.** Cyclic voltammograms in $Me_2SO$ (0.1 M TEAP) for $Mn^{III}(DTBC)_2(H_2O)_2^-$ and its reaction products when combined with $O_2^-$. The indicator electrode was a platinum disk (0.23 $cm^2$), and the scan rate was 0.1 V $s^{-1}$.

anaerobic conditions, the addition of 1 equiv of DTBQ to a solution of th red-brown species causes it to become blue with an absorption peak at 590 nm.

Figure 6 illustrates the cyclic voltammetry for $Mn^{III}(DTMC)_2^-$ in $Me_2SO$. The complex exhibits an initial reduction peak at −1.75 V vs. SCE and an initial oxidation peak at +0.2 V vs. SCE. When 1 equiv of superoxide ion is added to the green solution, it turns blue and has electrochemical characteristics that are similar to those for the $Mn^{IV}(DTBC)_3^{2-}$ complex. When excess is added to a solution of $Mn^{III}(DTBC)_2^-$, it becomes red-brown and its cyclic voltammogram has initial oxidation peaks at −0.40 V vs. SCE and −0.25 V; the latter yields a reduction peak at −0.85 V vs. SCE after scan reversal. When 1 equiv of DTBQ is added to this solution, its cyclic voltammogram is almost identical with that for the dioxygen adduct of $Mn^{IV}(DTBC)_3^{2-}$ (see Figure 7) and includes reduction peaks that are characteristic of free DTBQ and dissolved dioxygen. When this solution is purged with argon, the dioxygen peak disappears. Electrochemical measurements of this system in MeCN and DMF indicate that

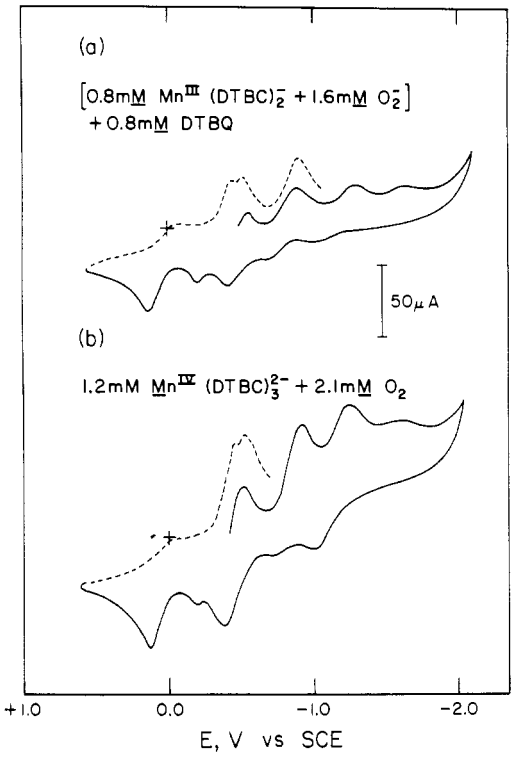


**Figure 7.** Cyclic voltammogram in $Me_2SO$ (0.1 M TEAP) for the $O_2$ adduct of 1 mM $Mn^{IV}(DTBC)_3^{2-}$ and for the product solution that results from the combination of 1 mM $Mn^{III}(DTBC)_2(H_2O)_2^-$ and 2 mM $O_2^-$ plus 1 mM DTBQ. The indicator electrode was a platinum disk (0.23 $cm^2$), and the scan rate was 0.1 V $s^{-1}$.

highly reactive intermediates are formed that attack the electrode surface; meaningful redox data are precluded.

The $Mn^{III}(DTBC)_2^-$ complex is ESR silent at 77 K. However, after the addition of 1 equiv of superoxide ion, a sharp resonance at $g = 2.0$ (line width ~2 G) is observed. When excess $O_2^-$ is added to $Mn^{III}(DTBC)_2^-$, the resulting brown solution exhibits the same ESR resonance at $g = 2.0$ plus a broader overlapping resonance (line width ~20 G). If this solution is stored in an inert-atmosphere box for a week, the broader signal disappears but the sharp resonance remains.

The $Mn^{IV}(DTBC)_3^{2-}$ complex is ESR silent at 77 K. After the addition of 1 equiv of $O_2^-$, a peak with a line width of ~20 G appears at $g = 2.0$. When an excess of $O_2^-$ is added to $Mn^{IV}(DTBC)_3^{2-}$, the same broad ESR resonance at $g = 2.0$ is observed plus a sharp overlapping resonance with a line width of ~2 G.

**Reactions of $Mn^{IV}(DTBC)_3^{2-}$ with Superoxide Ion.** When the blue $Mn^{IV}(DTBC)_3^{2-}$ complex is combined with 1 equiv of $O_2^-$ in MeCN, a red-brown species is formed with an absorption peak at 450 nm. The spectrum is essentially the same as that for the combination of $Mn^{III}(DTBC)_2^-$ and $O_2^-$ (Figure 5). In $Me_2SO$ a one-to-one ratio of $O_2^-$ and $Mn^{IV}(DTBC)_3^{2-}$ yields a bluish solution with an absorption peak at 460 nm. Excess superoxide ion causes the solution to become gray-green.

The cyclic voltammogram for the products from the combination of 2 equiv of $O_2^-$/equiv of $Mn^{IV}(DTBC)_3^{2-}$ in $Me_2SO$ exhibits an initial reduction peak at −1.14 V vs. SCE and initial oxidation peaks at −0.4 and −0.15 V, which give a reduction peak at −0.8 V after the scan is reversed (the voltammogram is similar to that of Figure 6b). Electrochemical studies of this system in MeCN and DMF are preculuded because the product species attack the electrode.

**Reversible Formation of the Dioxygen Adduct of $Mn^{IV}(DTBC)_3^{2-}$.** When dioxygen (at 1 atm) is bubbled through a MeCN solution that contains 0.1 mM $Mn^{IV}(DTBC)_3^{2-}$ and

Table IV. Magnetic Moments of 5–25 mM Solutions of $Mn^{IV}(DTBC)_3^{2-}$ and $Mn^{III}(DTBC)_2^-$ in $Me_2SO$-$d_6$ at 25 °C and Effective Moments per Manganese Ion for the Stoichiometric Combination of $O_2$ and $O_2^-$ (as $(TMA)O_2$) with the Complexes

| compd or combination | moment, $\mu_B$ |
|---|---|
| $Na_2Mn^{IV}(DTBC)_3 \cdot 6MeCN$ | 3.9 |
| $NaMn^{III}(DTBC)_2 \cdot 4MeCN$ | 5.1 |
| $NaMn^{III}(DTBC)_2 \cdot 4MeCN + O_2$ (1 atm) | 5.1 |
| $Na_2Mn^{IV}(DTBC)_3 \cdot 6MeCN + O_2$ (1 atm) | 3.3 |
| $NaMn^{III}(DTBC)_2 \cdot 4MeCN + 0.5O_2^-$ | 4.6 |
| $NaMn^{III}(DTBC)_2 \cdot 4MeCN + 1O_2^-$ | 4.1 |
| $NaMn^{III}(DTBC)_2 \cdot 4MeCN + 1.6O_2^-$ | 3.7 |
| $NaMn^{III}(DTBC)_2 \cdot 4MeCN + 2O_2^-$ | 3.9 |
| $NaMn^{III}(DTBC)_2 \cdot 4MeCN + 3O_2^-$ | 4.1 |
| $NaMn^{III}(DTBC)_2 \cdot 4MeCN + 4.8O_2^-$ | 4.1 |
| $NaMn^{III}(DTBC)_2 \cdot 4MeCN + 6O_2^-$ | 3.9 |
| $Na_2Mn^{IV}(DTBC)_3 \cdot 6MeCN + 1O_2^-$ | 2.9 |
| $Na_2Mn^{IV}(DTBC)_3 \cdot 6MeCN + 2O_2^-$ | 3.2 |
| $Na_2Mn^{IV}(DTBC)_3 \cdot 6MeCN + 3O_2^-$ | 3.3 |
| $Na_2Mn^{IV}(DTBC)_3 \cdot 6MeCN + 4O_2^-$ | 3.2 |

0.1 mM (TEA)OH or 0.1 mM NaOH, the blue solution changes to a red-brown color; the process is reversed by purging the system with Ar. The reversibility is enhanced at lower temperstures (<0 °C). Without $OH^-$ or at room temperature the dioxygen adduct decomposes rapidly to a yellow solution.

**Magnetic Susceptibility Measurements.** The Evans[19-22] NMR method has been used to determine the magnetic moments of $Mn^{IV}(DTBC)_3^{2-}$ and $Mn^{III}(DTBC)_2^-$ and of their $O_2^-$ and $O_2$ adducts in $Me_2SO$-$d_6$ solutions. These data are summarized in Table IV.

## Discussion and Conclusions

**Structural Features.** On the basis of the X-ray diffraction results, crystalline disodium tris(3,5-di-*tert*-butylcatecholato)manganate(IV) has a nearly symmetric octahedral array of six catechol oxygen atoms around a central manganese(IV) ion. The spectrophotometric, magnetic, and electrochemical data confirm that the complex retains its main structural features in solution.

Because the proton NMR spectrum for tris(3,5-di-*tert*-butylcatecholato)manganate(IV) has the phenyl H resonance shifted far out of the diamagnetic region, the paramagnetic manganese center exerts hyperfine interactions with its catechol ligands.[23] The shifts with temperature are small for the *tert*-butyl protons and large for the phenyl protons (Figure 4), but both follow the Curie law with a zero intercept at $T^{-1} = 0$.[24] This indicates that only one spin state is populated in the $Mn^{IV}(DTBC)_3^{2-}$ complex ($S = {}^3/_2$). The increase in shifts at lower temperature is characteristic of a paramagnetic center.[25,26] The NMR results for the $Mn^{IV}(DTBC)_3^{2-}$ complex also indicate that the *tert*-butyl proton resonances are shifted downfield while the phenyl protons are shifted upfield. The *tert*-butyl groups probably are insulated against the delocalization by the unpaired electrons of the paramagnetic manganese(IV) center. This implies that a major portion of the isotropic shift for the *tert*-butyl resonance is due to the dipolar interaction. Because the peak is only shifted slightly compared to the diamagnetic resonance, this dipolar interaction probably is weak. The weak dipolar interaction of the *tert*-butyl protons indicates that the susceptibility anisotropy ($\chi_\parallel - \chi_\perp$) is small.[24,27] Hence, the $Mn^{IV}(DTBC)_3^{2-}$ complex is almost magnetically isotropic. Molecules with strong *L–S* coupling usually exhibit large magnetic anisotropy.[28] Because of the small degree of anisotropy for the $Mn^{IV}(DTBC)_3^{2-}$ complex, its magnetic moment (3.9 $\mu_B$) is due mainly to a spin-only contribution from the $S = {}^3/_2$ spin state for the Mn(IV) ion. The dipolar interaction is small, which means that the large isotropic shift of the phenyl protons must be due to a contact shift. The latter is a function of the density of unpaired electrons at the observed protons.[23] A high density of unpaired spin at the phenyl protons is consistent with the delocalization of the $\pi$ electrons for aromatic systems such as the catechol ligand.

**Redox Reactions for $Mn^{IV}(DTBC)_3^{2-}$ and $Mn^{III}(DTBC)_2^-$.** The electrochemical and spectrophotometric results from a previous study[13] indicate that the $Mn^{IV}(DTBC)_3^{2-}$ complex undergoes an irreversible one-electron reduction in $Me_2SO$ (eq 1) and two irreversible oxidations (eq 2, 3).

$$Mn^{IV}(DTBC)_3^{2-} + e^- \rightarrow Mn^{III}(DTBC)_3^{3-} \xrightarrow{H_2O} Mn^{III}(DTBC)_2(OH)^{2-} + DTBCH^- \quad (1)$$

$$E_{p,c} = -1.2 \text{ V vs. SCE}$$

$$Mn^{IV}(DTBC)_3^{2-} \rightarrow Mn^{III}(DTBC)_2^- + DTBQ + e^- \quad (2)$$

$$E_{p,a} = -0.4 \text{ V vs. SCE}$$

$$Mn^{III}(DTBC)^{2-} \rightarrow Mn(II) + 2DTBQ + 3e^- \quad (3)$$

$$E_{p,a} = +0.2 \text{ V vs. SCE}$$

The present results indicate that the $Mn^{III}(DTBC)_2^-$ complex is extremely stable to reduction. Hence, a catalytic reduction of bound water (from the $Me_2SO$ solvent matrix) occurs (eq 4).

$$Mn^{III}(DTBC)_2(H_2O)_2^- + e^- \rightarrow Mn^{III}(DTBC)_2(OH)(H_2O)^{2-} + {}^1/_2H_2 \quad (4)$$

$$E_{p,c} = -1.75 \text{ V vs. SCE}$$

The oxidation process yields free quinone and Mn(II) (eq 5).

$$Mn^{III}(DTBC)_2(H_2O)_2^- \rightarrow Mn^{II}(H_2O)_2 + 2DTBQ + 3e^- \quad (5)$$

$$E_{p,a} = +0.2 \text{ V vs. SCE}$$

**Formation of $O_2^-$ Adducts.** The experimental results in the preceding section provide an indication of the reactivity of $O_2^-$ with the $Mn^{III}(DTBC)_2(H_2O)_2^-$ and $Mn^{IV}(DTBC)_3^{2-}$ complexes in MeCN, DMF, and $Me_2SO$. Combination of $O_2^-$ and $Mn^{IV}(DTBC)_3^{2-}$ results in the formation of a red-brown product:

$$Mn^{IV}(DTBC)_3^{2-} + O_2^- \rightarrow Mn^{III}(DTBC)_2(DTBSQ)(O_2^-)^{3-} \quad (6)$$

The cyclic voltammogram for this system exhibits a major oxidation peak at +1.0 V vs. SCE in $Me_2SO$, which is characteristic of a two-electron oxidation of bound DTBC.[29] The proposed product species has an experimental magnetic moment of 2.9 $\mu_B$ (Table IV), which is close to that for a two-unpaired-electron system (2.83 $\mu_B$). The absorption band at

(23) LaMar, G. N. "NMR of Paramagnetic Molecules"; LaMar, G. N., Horrocks, W. D., Jr., Holm, R. H., Eds.; Academic Press: New York, 1973; Chapter 3.
(24) Jesson, J. P. "NMR of Paramagnetic Molecules"; LaMar, G. N., Hoorocks, W. D., Jr., Holm, R. H., Eds.; Academic Press: New York, 1973; Chapter 1.
(25) LaMar, G. N.; Walker, F. A. *J. Am. Chem. Soc.* **1973**, *95*, 1782.
(26) LaMar, G. N.; Walker, F. A. *J. Am. Chem. Soc.* **1973**, *95*, 1790.
(27) Goff, H.; LaMar, G. N.; Reed, C. A. *J. Am. Chem. Soc.* **1977**, *99*, 3641.
(28) Chin, D.-H., Ph.D. Dissertation, Univeristy of California, Davis, CA, 1979.
(29) Chin, D.-H.; Jones, S. E.; Leon, L. E.; Bosserman, P.; Stallings, M. D.; Sawyer, D. T. *Adv. Chem. Ser.* **1982**, *201*, 675.

300 nm also is consistent with a Mn(III) center.[29] Likewise, the ESR spectrum for the product ($g = 2$, $A = 20$ G) indicates the presence of bound $DTBSQ^{-}\cdot$.

When excess $O_2^-$ is added to $Mn^{IV}(DTBC)_3^{2-}$, the magnetic moment of the solution increases and an additional sharp ESR resonance at $g = 2.0$ appears that is characteristic of free $DTBSQ^{-}\cdot$.

$$Mn^{IV}(DTBC)_3^{2-} + 2O_2^- \rightarrow Mn^{III}(DTBC)(DTBSQ)(O_2^-)(O_2^{2-})^{3-} + DTBSQ^{-}\cdot \quad (7)$$

In basic solution $O_2^-$ does not react with $Mn^{IV}(DTBC)_3^{2-}$.

The 1:1 combination of $O_2^-$ and the $Mn^{III}(DTBC)_2(H_2O)_2^-$ complex gives a transient red-brown adduct, which decomposes to $Mn^{IV}(DTBC)_3^{2-}$ and a Mn(III) complex:

$$Mn^{III}(DTBC)_2(H_2O)_2^- + O_2^- \rightarrow {}^2/_3Mn^{IV}(DTBC)_3^{2-} + {}^1/_3[Mn^{III}(O_2^{2-})_2(O_2^-)] \quad (8)$$

The 67% yield of $Mn^{IV}(DTBC)_3^{2-}$ is confirmed by the UV–visible spectra and electrochemistry for the product solution. On the basis of the magnetic moments (Table IV), the net spins of the product species are equivalent to three unpaired electrons. The appearance of an ESR resonance at $g = 2.0$ for the product solution probably is due to some $DTBSQ^{-}\cdot$ (bound or free).

When excess $O_2^-$ is added to $Mn^{III}(DTBC)(H_2O)_2^-$, a series of disproportionation reactions apparently occur with some oxygenation of $Me_2SO$ to give an $O_2^-$ adduct:

$$Mn^{III}(DTBC)_2(H_2O)_2^- + 3O_2^- + Me_2SO \rightarrow Mn^{III}(DTBC)_2(O_2^-)(OH)^{3-} + Me_2SO_2 + O_2 + OH^- + H_2O \quad (9)$$

The latter has an apparent magnetic moment of 4.1 $\mu_B$ (after the solution is deaerated with argon). Addition of 1 equiv of DTBQ to this product species yields $O_2$ and the blue $Mn^{IV}(DTBC)_3^{2-}$ complex:

$$Mn^{III}(DTBC)_2(O_2^-)(OH)^{3-} + DTBQ \rightleftharpoons Mn^{IV}(DTBC)_3^{2-} + O_2 + OH^- \quad (10)$$

Electrolytic oxidation at −0.2 V vs. SCE of the $Mn^{III}(DTBC)_2(O_2^-)(OH)^{3-}$ complex also yields dioxygen and the green $Mn^{III}(DTBC)_2(H_2O)_2^-$ complex:

$$Mn^{III}(DTBC)_2(OH)(O_2^-)^{3-} \xrightarrow{H_2O} Mn^{III}(DTBC)_2(H_2O)_2^- + O_2 + OH^- + e^- \quad (11)$$

Three considerations, plus the spectroscopic and magnetic measurements for the $O_2$–$Mn^{IV}(DTBC)_3^{2-}$ system in basic MeCN, support the proposition that the reversible dioxygen adduct has the formula $Mn^{III}(DTBC)(DTBSQ)_2(O_2^-)(OH)^{3-}$ with an octahedral configuration:

$$Mn^{IV}(DTBC)_3^{2-} + O_2 + OH^- \rightleftharpoons Mn^{III}(DTBC)(DTBSQ)_2(O_2^-)(OH)^{3-} \rightarrow Mn^{III}(DTBC)_2(O_2^-)(OH)^{3-} + DTBQ \quad (12)$$

Although $Mn^{IV}(DTBC)_2(DTBSQ)(O_2^-)^{2-}$ was concluded to be the dominant form of the adduct in a previous study,[11] this is not consistent with the observed magnetic susceptibility, the apparent presence of the free DTBQ, and a solution color that is characteristic of manganese(III)–($O_2^-$) adducts. Apparently, such a species is subject to chemical (by $Me_2SO$, eq 9) and thermal degradation (eq 13). The presence of $DTBSQ^{-}\cdot$ and

$$Mn^{IV}(DTBC)_2(DTBSQ)(O_2^-)^{2-} \xrightarrow{OH^-} Mn^{III}(DTBC)_2(OH)_2^{3-} + DTBSQ^{-}\cdot + O_2 \quad (13)$$

DTBQ as intermediates and products is confirmed by the electrochemistry and the ESR spectra for this system. A positive electrochemicl scan for the product solution of reaction 12 yields an oxidation peak at −0.2 V vs. SCE, which results in a reduction peak at −0.85 V v. SCE upon scan reversal. Because $O_2$ is reduced at −0.85 V and this peak is removed by argon purging of the electrolyzed solution, there is compelling evidence that the product species of eq 12 contains a coordinated dioxygen species ($O_2^-$) that is oxidized at−0.2 V vs. SCE:

$$Mn^{III}(DTBC)_2(OH)(O_2^-)^{3-} \rightarrow Mn^{III}(DTBC)_2(OH)^{2-} + O_2 + e^- \quad (14)$$

Although reactions 6–14 are believed to be reasonable and self-consistent, the manganese–DTBC–$O_2$–$O_2^-$ systems are subject to a variety of hydrolytic, redox, and oligomeric equilibria. There clearly are other species in the various reactant combinations.

**Acknowledgment.** This work was supported by the USPHS—National Institutes of Health under Grants GM-22761 (D.T.S.) and HL-12395 (W.P.S.) and by the USDA—U.S. Forest Service under Agreement No. 12-167 (D.T.S.). We are grateful to Stephen Jones and to Thomas Calderwood of the University of California, Riverside, for helpful discussions and assistance with the electrochemical measurements and for the synthesis of $(TMA)O_2$. We appreciate the continuing advice and counsel of Richard E. Marsh of the California Institute of Technology.

**Registry No.** $Na_2Mn^{IV}(DTBC)_3 \cdot 6MeCN$, 84130-37-0; $Na-Mn^{III}(DTBC)_2$, 84130-38-1; $O_2^-$, 11062-77-4; $Mn^{III}(DTBC)_2(DTBSQ)(O_2^-)^{3-}$, 84130-39-2; $Mn^{III}(DTBC)(DTBSQ)(O_2^-)(O_2^{2-})^{3-}$, 84130-40-5; $Mn^{III}(DTBC)_2(O_2^-)(OH)^{3-}$, 84130-41-6; $Mn^{III}(DTBC)_2(H_2O)_2^-$, 84130-42-7.

**Supplementary Material Available:** Tables of anisotropic thermal parameters, assigned hydrogen parameters, and structure factor amplitudes (21 pages). Ordering information is given on any current masthead page.